



# Immobilized Cu–Cr layered double hydroxide films with visible-light responsive photocatalysis for organic pollutants

Lei Tian, Yufei Zhao, Shan He, Min Wei\*, Xue Duan

State Key Laboratory of Chemical Resource Engineering, Beijing University of Chemical Technology, Beijing 100029, China

## ARTICLE INFO

### Article history:

Received 1 October 2011  
Received in revised form 2 January 2012  
Accepted 14 January 2012

### Keywords:

Layered double hydroxides  
Film  
Photocatalysis  
Visible-light

## ABSTRACT

Oriented Cu–Cr layered double hydroxide (LDH) films have been fabricated by the electrophoretic deposition method (EPD) on copper substrates, which can be used as photocatalysts for the degradation of organic pollutants under visible-light irradiation. Powder X-ray diffraction (PXRD), scanning electron microscope (SEM), Fourier transform infrared (FT-IR) and Brunauer–Emmett–Teller (BET) reveal that the resulting CuCr-LDH film possesses high crystallinity, porous structure as well as large specific surface area. UV–vis diffuse reflection spectroscopy (DRS) confirms that the CuCr-LDH film shows a broad absorption in visible light region (>400 nm). The LDH film thickness can be controlled precisely by adjusting voltage or time of EPD. The film with thickness of 16.5  $\mu\text{m}$  shows excellent photocatalytic activity for the degradation of 2,4,6-trichlorophenol (2,4,6-TCP), sulforhodamine B (SRB) and Congo red. The photocatalytic reaction kinetics of 2,4,6-TCP was appropriately described by the pseudo-first-order model. In addition, the LDH film exhibits excellent recycleability compared with the corresponding powder sample, which facilitates its repeatable and cyclic usage over a long period. Owing to the high efficiency, low-cost preparation, easy manipulation and recyclability, it is expected that this film can be potentially used as photocatalyst in the field of water treatment.

© 2012 Elsevier B.V. All rights reserved.

## 1. Introduction

Environmental pollution and destruction on a global scale have drawn attention to the vital need for totally new, safe and clean chemical technologies and processes [1–5]. Many common industrial organic compounds that make their way into water systems can be carcinogenic at trace levels and are difficult and costly to remove completely with conventional technologies. Therefore various new technologies including physical, chemical and biological methods have been developed to deal with organic pollutants [6–9]. Among them, the photocatalytic oxidation process using heterogeneous photocatalysts is regarded as a promising technology to decompose harmful pollutants to final non-toxic products [10–12]. However, the majority of the commonly used photocatalysts (for instance,  $\text{TiO}_2$  and  $\text{ZnO}$ ) only can be activated under UV-light irradiation because of their large band gap, resulting in a low photo-electronic transition efficiency since the ultraviolet light is only 4% in solar spectrum [13,14]. Therefore, taking into account energy conservation and environmental pollution issue, it is necessary and desirable to develop visible light-driven photocatalysts with high efficiency.

Layered double hydroxides (LDHs) are inorganic layered anionic clays generally expressed by the formula  $[\text{M}^{\text{II}}_{1-x}\text{M}^{\text{III}}_x(\text{OH})_2] (\text{A}^{n-})_{x/n} \cdot m\text{H}_2\text{O}$  ( $\text{M}^{\text{II}}$  divalent and  $\text{M}^{\text{III}}$  trivalent metals, respectively,  $\text{A}^{n-}$   $n$  valent anion), which have been widely used in adsorption, separation and catalysis [15–19]. In recent years, LDHs have received great attention in photocatalysis as they show high selectivity and good stability [20–22]. For example, Garcia and co-workers reported that the ZnM-LDH ( $\text{M}=\text{Cr}, \text{Ti}, \text{Ce}$ ) serve as “doped semiconductors” for the visible-responsive photocatalysis of oxygen generation from water [23]. As for the LDH powder photocatalysts however, the aggregation as well as difficulties in operation, separation and recovery remain serious problems which limit their practical applications. From this point of view, immobilized LDH films with micro- and nano-features have evoked considerable interest due to the high dispersion of LDH microcrystals, easy manipulation and regeneration. Many approaches have been reported for the preparation of LDH films, including the solvent evaporation [24], hydrolysis of alkoxide [25], ultrasonication [26], co-precipitation [27], layer-by-layer assembly [28] and *in situ* growth on aluminium substrate [29]. Recently, our group reported the preparation of LDH films *via* the sol–gel and electrophoretic deposition method (EPD) method to adsorb toxic pollutants in water treatment [15,30]. However, very few reports were focused on the photocatalytic performance of LDH films. This motivates us to further study the semiconductor property and resulting photocatalytic behavior of LDH film materials, for the purpose of

\* Corresponding author. Tel.: +86 10 64412131; fax: +86 10 64425385.  
E-mail addresses: [weimin@mail.buct.edu.cn](mailto:weimin@mail.buct.edu.cn), [weimin-hewei@163.com](mailto:weimin-hewei@163.com) (M. Wei).

obtaining immobilized and recyclable photocatalysts for water treatment.

In this work, Cu–Cr layered double hydroxide (CuCr-LDH) film was immobilized on copper substrates by the method of electrophoretic deposition, and their visible-light-driven photocatalysis for the degradation of organic pollutants (2,4,6-TCP, SRB and Congo red) in water was successfully demonstrated. The LDH film thickness can be controlled precisely by adjusting voltage or time of EPD, and the film with thickness of 16.5  $\mu\text{m}$  shows excellent photocatalytic activity for the decomposition of the three organic contaminants (2,4,6-TCP, SRB and Congo red). The pseudo-first-order model can be used to describe the photocatalytic reaction kinetics of 2,4,6-TCP. The LDH film exhibits superior photocatalytic activity, pronounced recyclability and convenient manipulation compared with the powder sample. Therefore, this work provides a facile and effective approach for the preparation of visible-light-driven CuCr-LDH film photocatalyst, which can be applied in water treatment with low cost and long-term usage.

## 2. Experimental

### 2.1. Materials

Analytical grade chemicals including  $\text{Cu}(\text{NO}_3)_2 \cdot 3\text{H}_2\text{O}$ ,  $\text{Cr}(\text{NO}_3)_3 \cdot 9\text{H}_2\text{O}$ , NaOH, ethanol were purchased from the Beijing Chemical Co. Ltd. and used without further purification. The deionized and decarbonated water was used in all the preparation processes. 2,4,6-TCP, SRB and Congo Red were obtained from Sigma Chemical. Co. Ltd.

### 2.2. Synthesis of CuCr-LDH

Solution A:  $\text{Cu}(\text{NO}_3)_2 \cdot 3\text{H}_2\text{O}$  and  $\text{Cr}(\text{NO}_3)_3 \cdot 9\text{H}_2\text{O}$  with  $\text{Cu}^{2+}/\text{Cr}^{3+}$  molar ratio of 2.0, were dissolved in deionized water (100 ml) to give a solution with  $\text{Cu}^{2+}$  concentration of 0.5 M. Solution B: NaOH was dissolved in deionized water (100 ml) to form a 1.5 M basic solution. Solution A (100 ml) and solution B (100 ml) were simultaneously added to a colloid mill [31] rotating at 3000 rpm and mixed for 1.5 min. The resulting slurry was removed from the colloid mill and aged at 120 °C for 24 h. The final precipitate was filtered, washed thoroughly with deionized water, and dried at 65 °C for 12 h.

### 2.3. Preparation of CuCr-LDH film by the EPD

Copper foils were polished by sand paper to remove the oxide layer and ultrasonically treated in ethanol and deionized water respectively, prior to deposition of the LDH film. Electrophoretic deposition of  $\text{Cu}_2\text{Cr}-\text{NO}_3$ -LDH was performed in a cuboid glass cell with a copper foil as anode and another copper foil as a counter electrode connected to a DC power supply through the ammeter. The electrodes were fixed in parallel to each other with a distance of 3 cm. The voltage and deposition time can be controlled precisely. The LDH films immobilized on the surface of working electrode were washed by water and dried in air at room temperature overnight.

### 2.4. Characterization

Powder X-ray diffraction (PXRD) of CuCr-LDH samples were collected on a Shimadzu XRD-6000 diffractometer using a  $\text{Cu K}\alpha$  source, with a scan step of 0.02° and a scan range between 3° and 70°. The Fourier transform infrared (FT-IR) spectra were obtained using a Vector 22 (Bruker) spectrophotometer with 2  $\text{cm}^{-1}$  resolution. Solid-state UV–vis diffuse reflectance spectra were recorded in air at room temperature by means of a Beijing

PGENERAL TU-1901 spectrometer equipped with an integrating sphere attachment using  $\text{BaSO}_4$  as background. The morphology of the CuCr-LDH film was investigated using a scanning electron microscopy (SEM; Zeiss Supra 55) with an accelerating voltage of 20 kV. The specific surface area determination and pore volume and size analysis were performed by Brunauer–Emmett–Teller (BET) and Barrett–Joyner–Halender (BJH) methods using a Quantachrome Autosorb-1C-VP Analyzer. Prior to the measurements, the samples were degassed at 120 °C for 5 h. The porosity of the film sample was measured by scratching the CuCr-LDH film from the substrate carefully, and the powder sample obtained by the co-precipitation method was also measured for comparison. The content of total chromium in the solution after reaction was measured by inductively coupled plasma (ICP) emission spectroscopy (Shimadzu ICPS-7500).

### 2.5. Photocatalytic reaction

The photocatalytic activity of CuCr-LDH film was monitored by degradation of 2,4,6-TCP, SRB and Congo red respectively. The visible-light irradiation source was a 300 W xenon lamp (CEL-HXBF300, Beijing AuLight Co. Ltd.) equipped with a wavelength pass filter ( $\lambda > 400 \text{ nm}$ ). The schematic diagram of photocatalytic reactor is shown in Fig. S1. Experiment was performed by anchoring the films with 100 mg of catalyst in a silica dish containing 20 ml of 2,4,6-TCP (30 ppm), SRB (50 ppm) or Congo red (100 ppm) solution which was stirred magnetically. The pH of the solutions remains at 6.8, 7.0 and 6.6 respectively without obvious change during the photocatalytic process. At first, the reactants were vigorously stirred for 30 min in the dark to establish an adsorption/desorption equilibrium; then the reaction occurred under visible-light irradiation. 3 ml of aliquots were sampled for analysis at given time intervals, which were reused in the subsequent reaction. The samples were analyzed by measuring the absorption band maximum (295 nm for 2,4,6-TCP, 565 nm for SRB and 500 nm for Congo red) using a Beijing PGENERAL TU-1901 UV–vis spectrophotometer. The blank reaction was carried out following the same procedure without adding catalyst.

## 3. Results and discussion

### 3.1. Characterization of the LDH films

Fig. 1a displays the XRD pattern of CuCr-LDH powder sample ( $\text{Cu}^{2+}/\text{Cr}^{3+}$  molar ratio of 2:1), from which the reflections of (003), (006), (012) and (110) indexed to typical LDH materials were observed, with a basal spacing of 0.888 nm. This is in accordance with  $\text{NO}_3$ -type LDHs. Comparison of the CuCr-LDH films by the EPD method (Fig. 1b–e and Fig. S2) with the LDH powder sample (Fig. 1a) only shows the presence of (003) reflection for the film sample, indicating a highly ordered stacking of the *ab* plane of LDH platelets parallel to the substrate [24,32]. The two strong reflections are attributed to the (111) and (200) from the Cu substrate (Fig. 1b–e and Fig. S2). The FT-IR technique was also used to identify the nature and symmetry of interlayer anions (see Fig. S3a). The spectrum of the CuCr-LDH powder sample shows the characteristic  $\nu_3$  band of  $\text{NO}_3^-$  at 1382  $\text{cm}^{-1}$ ; while the broad absorption at  $\sim 3400 \text{ cm}^{-1}$  is due to stretching mode of hydrogen-bonded hydroxyl groups in both the brucite-like layers and the interlayer water molecules [33]. The UV–vis diffuse reflectance spectrum of CuCr-LDH powder sample (Fig. 2) shows the appearance of two broad absorption bands in the visible region at  $\sim 410$  and 570 nm, which can be respectively attributed to the d–d transition  ${}^4\text{A}_{2g}(\text{F}) \rightarrow {}^4\text{T}_{1g}(\text{F})$  and  ${}^4\text{A}_{2g}(\text{F}) \rightarrow {}^4\text{T}_{2g}(\text{F})$  of  $\text{Cr}^{3+}$  in an octahedral environment in the LDH layer [34,35]. The broad absorption of CuCr-LDH material motivates

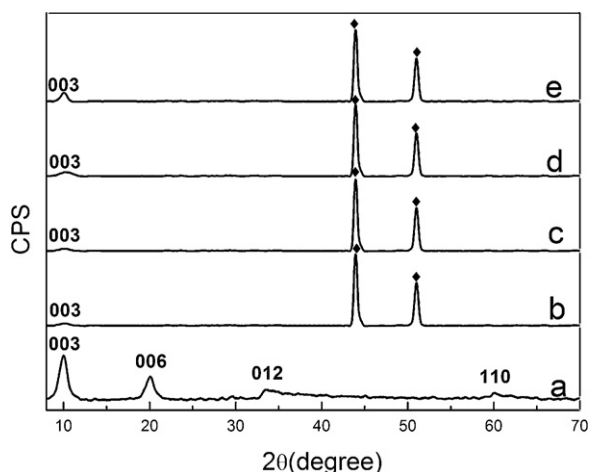


**Fig. 1.** XRD patterns for the CuCr-LDH powder sample (a) and CuCr-LDH film samples at different EPD voltage for 10 min: (b) 10 V; (c) 30 V; (d) 50 V; (e) 70 V. The rhombic symbol indicates the (111) and (200) reflections from the copper substrate.

us to explore their potential visible-light photocatalytic activity in the following section.

The morphology of films prepared *via* the EPD method by immobilizing CuCr-LDH powder suspension onto copper substrate is shown in Fig. 3 and supporting information Fig. S4–S6. As shown in Fig. 3, the film thickness (2.5–27.0 μm) increases gradually along with the increase of electrophoresis voltage (10–70 V). Moreover, the film thickness can be also precisely controlled by changing the electrophoresis time: the thickness increases from 3.0 to 6.5 μm by prolonging the electrophoresis time from 3 to 12 min at 50 V (Fig. S4). In addition, abundant porous fabrication of the film (Supporting Information Figs. S5 and S6) imposes great influence

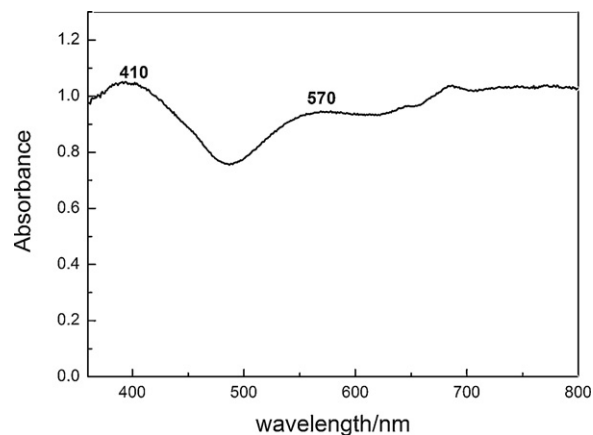


**Fig. 2.** The UV-vis diffuse reflectance spectrum of CuCr-LDH powder sample.

on the adsorption and photodegradation of pollutants, which will be further discussed below.

### 3.2. Photocatalytic activity of the CuCr-LDH film

The visible-light photocatalytic activity of the as-prepared CuCr-LDH film samples was studied *via* the degradation of 2,4,6-TCP. The absorption spectra of the solution as a function of irradiation time during the degradation process (at every 20 min interval over a period of 200 min for 2,4,6-TCP) were recorded by using a UV-vis spectrometer (Fig. 4). The self-degradation of 2,4,6-TCP was also studied, and only ~5% of 2,4,6-TCP was photolyzed after 200 min irradiation without any catalyst. The photodegradation of 2,4,6-TCP was enhanced remarkably with the presence of CuCr-LDH powder sample, *i.e.*, ~47% of 2,4,6-TCP was degraded after 200 min irradiation. In the case of the film sample, it can be seen that the film

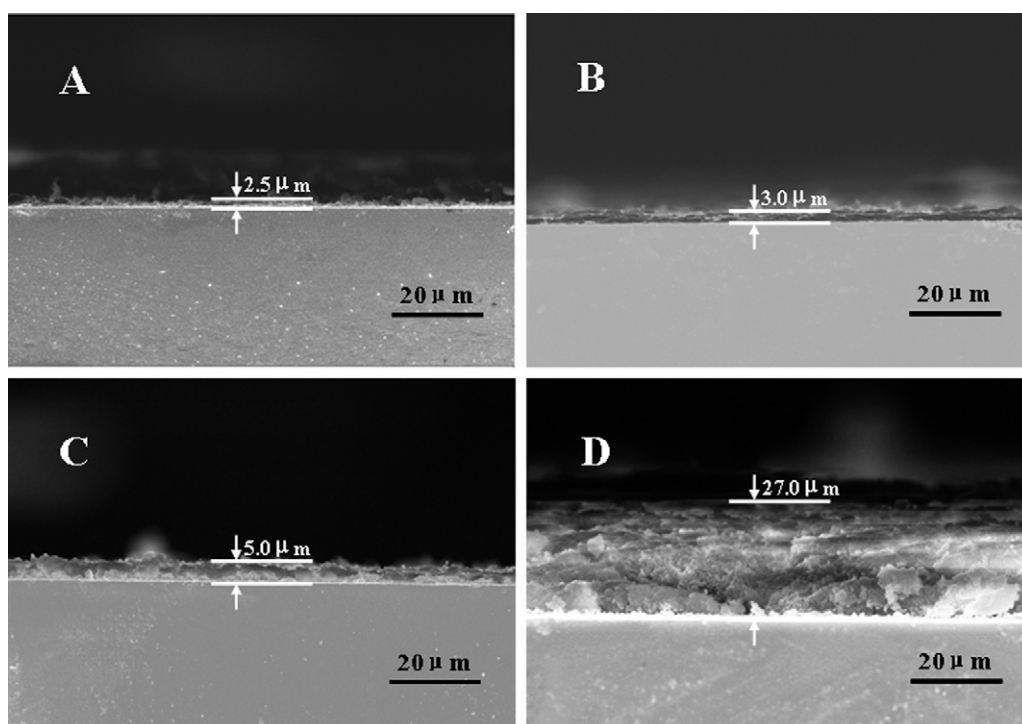


**Fig. 3.** Side-view of SEM images for CuCr-LDH film samples with different EPD voltage for 10 min: (A) 10 V; (B) 30 V; (C) 50 V; (D) 70 V.

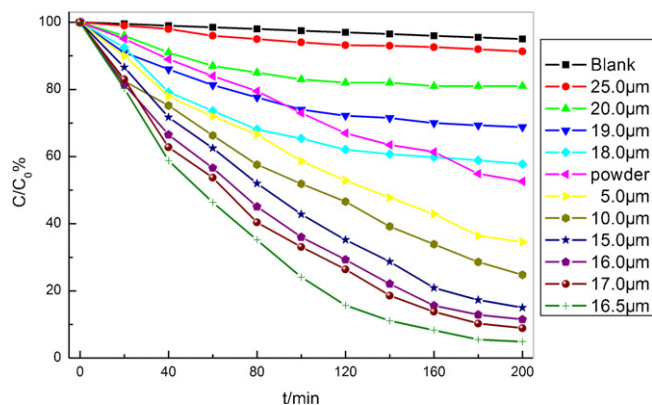


**Fig. 4.** Photodegradation of 2,4,6-TCP monitored as the normalized concentration vs irradiation time under visible-light irradiation ( $\lambda > 400$  nm) with the presence of LDH powder as well as film catalysts with different thickness.

thickness plays a key role in determining its photocatalytic activity. The photocatalytic activity of CuCr-LDH film enhanced along with the increase of film thickness from 5.0 to 16.5  $\mu\text{m}$ ; while a decrease in activity was observed with further increase of thickness in the range 16.5–25.0  $\mu\text{m}$ . The highest activity was obtained for the LDH film with the thickness of 16.5  $\mu\text{m}$ : 95% degradation of 2,4,6-TCP occurred in 200 min. The results indicate that the thickness and texture of the catalyst film affect its photocatalytic behavior significantly. In addition, the FT-IR spectrum of used catalyst (Fig. S3b) does not show the characteristic bands of 2,4,6-TCP (Fig. S3c), which indicates that the organic contaminant undergoes photodegradation rather than being adsorbed onto the surface of LDH film.

To give a further insight into the influence of film thickness and texture on the photocatalytic activity, four CuCr-LDH film samples with different thickness (5.0, 16.5, 18.0 and 25.0  $\mu\text{m}$ ) were chosen to have a further study. The UV–vis diffuse reflectance spectra of the CuCr-LDH films with different thickness (Fig. S7) show similar absorption behavior to the powder sample (Fig. 2). The porosity and specific surface area of the CuCr-LDH films (Fig. 5) and powder sample (Fig. S8) were further studied by nitrogen sorption measurements. According to BDDT (Brunauer–Deming–Deming–Teller) classification, all the samples display type IV isotherms with H3 type hysteresis loops. The powder sample (Fig. S8) shows uniform mesopores (3–5 nm), as a result of the accumulation of LDH particles. A broad pore-size distribution is observed for the LDH film samples with thickness of 5.0 and 16.5  $\mu\text{m}$ , but it turns to narrow for thicker films (18.0 and 25.0  $\mu\text{m}$ ). Table 1 lists that the LDH film (16.5  $\mu\text{m}$ ) shows the largest specific surface area, pore volume as well as diameter. Furthermore, Fig. S9 shows that the CuCr-LDH film becomes looser and more porous with the increase of thickness from 5.0 to 16.5  $\mu\text{m}$ ; while a dense stacking is observed accompanied with the disappearance of porosity as the film thickness increases to 18.0 and 25.0  $\mu\text{m}$ . Therefore, the specific architecture of the CuCr-LDH film (16.5  $\mu\text{m}$ ) offers a high specific surface area as well as suitable pore-size distribution,

**Table 1**  
BET surface area, pore volume and mean pore diameter of the CuCr-LDH powder and film samples.

Sample	BET surface area ( $\text{m}^2 \text{g}^{-1}$ )	Pore volume ( $\text{cm}^3 \text{g}^{-1}$ )	Mean pore diameter (nm)
LDH powder	67.4	0.117	6.94
5.0 $\mu\text{m}$ LDH film	157.9	0.301	7.64
16.5 $\mu\text{m}$ LDH film	187.8	0.599	12.75
18.0 $\mu\text{m}$ LDH film	79.3	0.127	6.43
25.0 $\mu\text{m}$ LDH film	61.4	0.111	7.25

accounting for the highest photocatalytic activity. Additionally, it is obvious that the LDH film (16.5  $\mu\text{m}$ ) exhibits a much better photocatalytic performance for 2,4,6-TCP compared with the powder sample. The poor photocatalytic activity of the LDH powder sample is probably due to its aggregation, which is generally inevitable for nanoparticles. In contrast, well *c*-oriented assemblies of LDH microcrystals on copper substrate (Fig. S10) as well as the porous film structure provide rich pores and large specific surface area, resulting in its largely improved photocatalytic activity. It has been reported that the photocatalytic efficiency can be greatly enhanced by increasing surface area, and a proper spatial arrangement further assists the electron/energy transfer within a porous framework [36].

### 3.3. Kinetics studies

The photodegradation kinetics was further studied to understand the reaction characteristic of 2,4,6-TCP on the LDH film. The linear relationship between  $\ln(C_0/C_t)$  and irradiation time (Fig. 6) suggests that the degradation of 2,4,6-TCP by the LDH film photocatalyst (16.5  $\mu\text{m}$ ) follows the pseudo first-order kinetics which could be described by the following equation:  $\ln(C_0/C_t) = kt$ , where  $C_0$  is the initial concentration and  $C_t$  is the concentration at time  $t$ . The apparent rate constant  $k$  of the film and powder sample was calculated to be  $0.0161 \text{ min}^{-1}$  ( $R^2 = 0.997$ ) and  $0.0033 \text{ min}^{-1}$  ( $R^2 = 0.998$ ), respectively. Half-life ( $t_{1/2}$ ) of the film and powder sample was found to be 43.1 min and 210.0 min respectively, which was calculated from  $k$  by using the equation:  $t_{1/2} = \ln 2/k$ . As a result, the photodegradation kinetics fitted well with the pseudo first-order model, indicating that the reaction rate is dependent on the light intensity and absorption performance of the catalyst [37].

### 3.4. Recycling ability of the LDH film catalysts

Because the recycling of photocatalysts is the most difficult and expensive part of photocatalytic technologies, a successful recycling process is very important to gain an efficient and low-cost technique for wastewater treatment systems. The recycle application of the LDH film photocatalyst was demonstrated by the decomposition of 2,4,6-TCP, SRB and Congo red respectively. Fig. 7, Figs. S11 and S12 display the degradation ratio of 2,4,6-TCP, SRB and Congo red vs cycle number for the LDH film and powder catalyst, respectively. As shown in Fig. 7, the degradation ratio of 2,4,6-TCP by the LDH powder sample in the first cycle was 88%, but it decreased very quickly and only 36% was obtained in the sixth reuse. In contrast, the film catalyst not only shows higher initial degradation ratio (97%) but also maintains at a high value (92%) in the consecutive cycles of photodegradation. Similarly, it can be observed that the photocatalytic activity of the LDH film for the decomposition of SRB and Congo red still keeps above 90% in the sixth cycle, while it decreases sharply for the corresponding powder sample (Fig. S11 and S12). Additionally, the XRD patterns (Fig. 8) show that the basal spacing ( $d_{003}$ ) of the LDH film decreases from 0.888 nm (Fig. 8a, the freshly prepared  $\text{NO}_3^-$ -LDH) to 0.735 nm (Fig. 8b, after the first cycle) which accords with carbonate-containing LDHs [38]. This compressed interlayer distance remains unchanged during the following cycles (Fig. 8c). The results indicate that carbonate was intercalated into LDH gallery during the photocatalytic reaction process, due to the particularly high affinity between carbonate and LDH host layer. Furthermore, this transformation was verified by the FT-IR spectroscopy (Fig. S3b), from which bands at 1384 and  $1352 \text{ cm}^{-1}$  attributed to the  $\nu_3$  peak splitting of  $\text{CO}_3^{2-}$  were observed. For the powder sample, serious aggregation of LDH particles may occur during the reuse process (Fig. S13A and B),

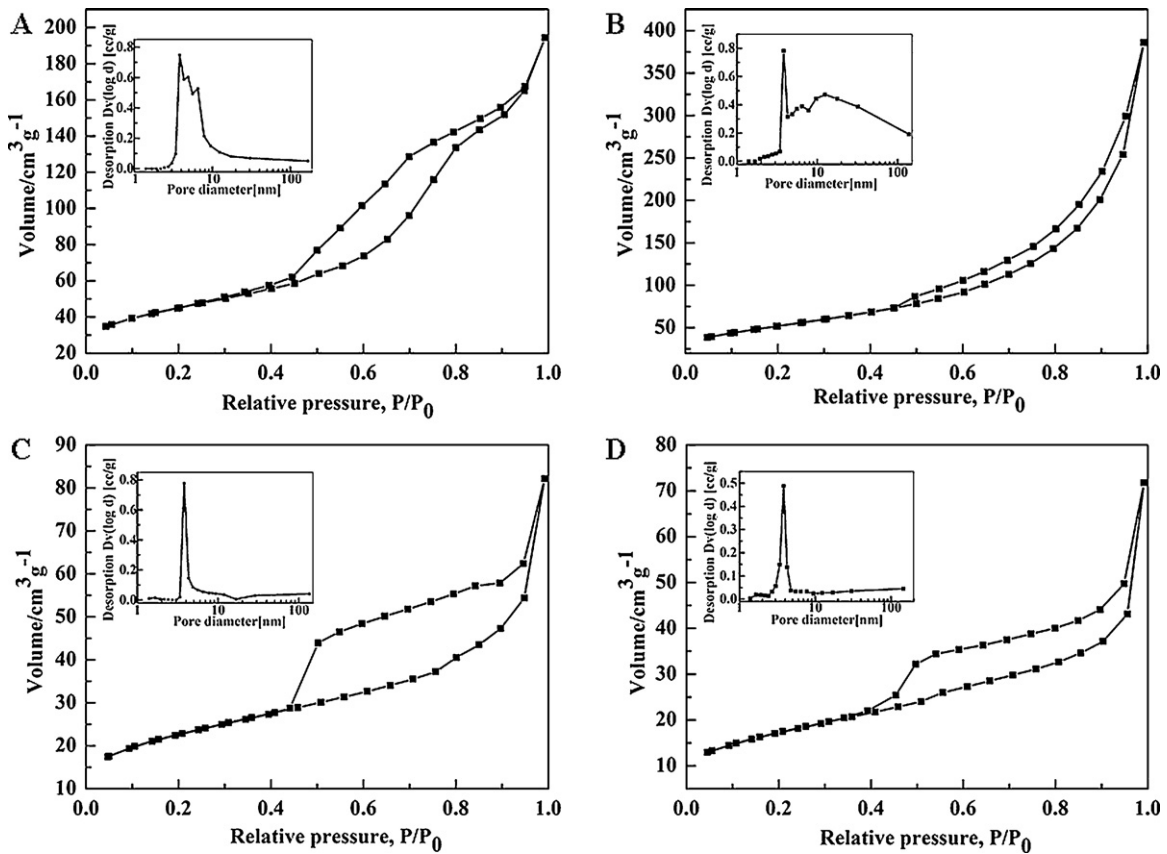


**Fig. 5.** Nitrogen adsorption–desorption isotherms of CuCr-LDH film samples with various thickness: (A) 5.0  $\mu\text{m}$ ; (B) 16.5  $\mu\text{m}$ ; (C) 18.0  $\mu\text{m}$ ; (D) 25.0  $\mu\text{m}$ . Inset: the corresponding pore-size distribution.

which imposes great influence on its photocatalytic behavior. The regeneration and recycling of the powder catalyst are frequently impracticable due to the irreversible adsorption of some intermediate compounds [39]. Compared with the powder sample, the superior photocatalytic recyclability of the LDH film can be attributed to the oriented packing of LDH particles with abundant meso-porous structure; moreover, no obvious change in its morphology was observed from SEM images after six reaction cycles (Fig. S13C and D).

The stability of the LDH film was also studied from the viewpoint of practical application. No delamination or peeling occurred

on cross-cutting the film surface, indicating a strong adhesion of the film to the substrate (Fig. S14). Furthermore, the leaching of chromium from the film or powder sample was tested. The chromium concentration in the solution after six reaction cycles was 12.9 ppm for the powder sample; whereas only 0.076 ppm was found for the film sample, indicating a strong stability of the LDH film. The results suggest that the LDH film can serve as a stable, effective and recyclable photocatalyst.

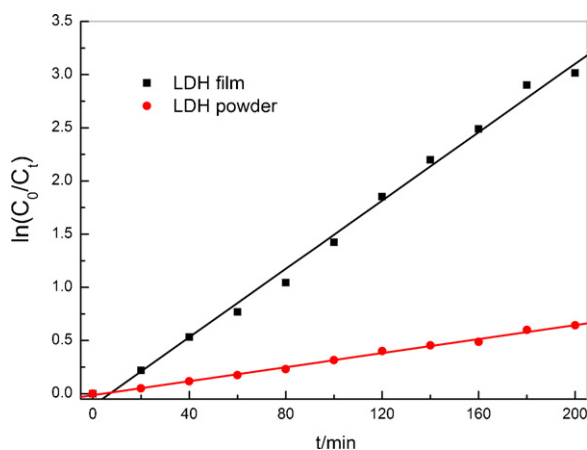


**Fig. 6.** First-order kinetics for the 2,4,6-TCP photodegradation by using the LDH film and powder catalyst respectively.

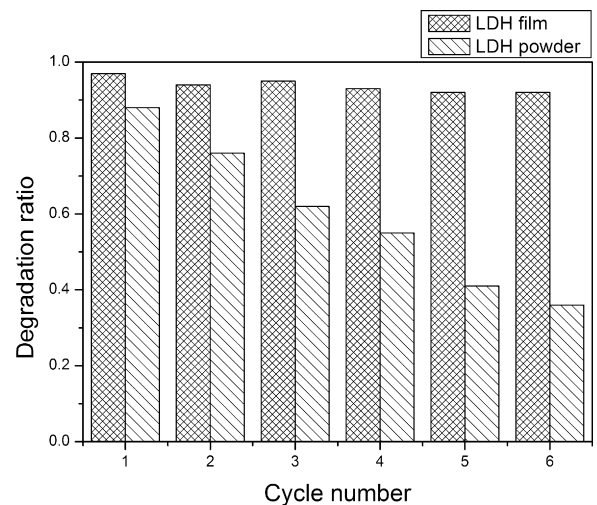


**Fig. 7.** Degradation ratio of 2,4,6-TCP solution vs. cycle number with the presence of LDH film and powder catalyst.

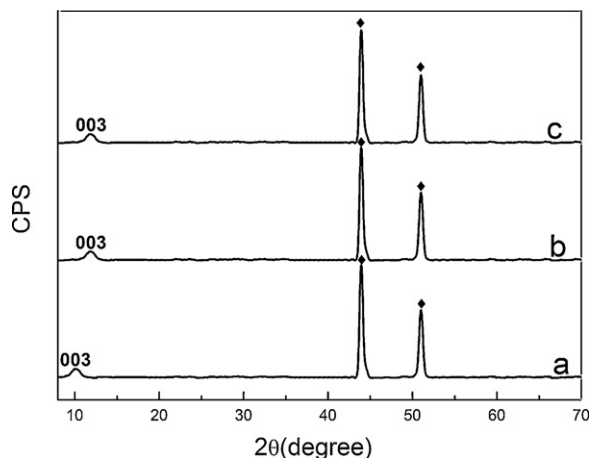


**Fig. 8.** XRD patterns of (a) the as-prepared CuCr-LDH film, (b) the CuCr-LDH film after one reaction cycle and (c) after six cycles. The rhombic symbol indicates the (1 1 1) and (2 0 0) reflection from the copper substrate.

#### 4. Conclusion

In summary, the CuCr-LDH films were prepared by the EPD method, which show a high *c*-orientation of the LDH platelets and strong adhesion to the substrate. The immobilized LDH films exhibit effective photocatalytic activity in the visible part of the solar spectrum for the degradation of 2,4,6-TCP, SRB and Congo red. The film thickness can be controlled accurately by adjusting the voltage and time of EPD. The LDH film with the thickness of 16.5  $\mu\text{m}$  shows superior photocatalytic activity for 2,4,6-TCP compared with the corresponding LDH powder sample, due to its large specific area and the rich macro-/meso-porous structure. The photocatalytic reaction kinetics is satisfactorily described by the pseudo-first-order model. In addition, the film catalyst exhibits excellent photocatalytic stability and recyclability, facilitating its repeatable and cyclic usage over a long period. It is expected that the immobilized LDH film in this work can be potentially used as an effective and recyclable visible-light-driven photocatalyst for large-scale water treatment.

#### Acknowledgements

This work was supported by the the 863 Program (grant no.: 2009AA064201), the National Natural Science Foundation of China, the 111 Project (grant no.: B07004) and the Collaboration Project from the Beijing Education Committee.

#### Appendix A. Supplementary data

Supplementary data associated with this article can be found, in the online version, at [doi:10.1016/j.cej.2012.01.070](https://doi.org/10.1016/j.cej.2012.01.070).

#### References

- [1] A.L. Linsebigler, G. Lu, J.T. Yates Jr., Photocatalysis on  $\text{TiO}_2$  surfaces: principles, mechanisms, and selected results, *Chem. Rev.* 95 (1995) 735–758.
- [2] M.R. Hoffmann, S.T. Martin, W.Y. Choi, D.W. Bahnemann, Environmental applications of semiconductor photocatalysis, *Chem. Rev.* 95 (1995) 69–96.
- [3] C.C. Chen, W.H. Ma, J.C. Zhao, Semiconductor-mediated photodegradation of pollutants under visible-light irradiation, *Chem. Soc. Rev.* 39 (2010) 4206–4219.
- [4] M. Zhang, Q. Wang, C.C. Chen, L. Zang, W.H. Ma, J.C. Zhao, Oxygen atom transfer in the photocatalytic oxidation of alcohols by  $\text{TiO}_2$ : oxygen isotope studies, *Angew. Chem.* 121 (2009) 6197–6200.
- [5] Y. Xu, C.H. Langford, UV- or visible-light-induced degradation of X3B on  $\text{TiO}_2$  nanoparticles: the influence of adsorption, *Langmuir* 17 (2001) 897–902.
- [6] P. Nigam, G. Armour, I.M. Banat, D. Singh, R. Marchant, Physical removal of textile dyes and solid-state fermentation of dye-adsorbed agricultural residues, *Bioresour. Technol.* 72 (2000) 219–226.
- [7] G. Moussavi, M. Mahmoudi, Degradation and biodegradability improvement of the reactive red 198 azo dye using catalytic ozonation with MgO nanocrystals, *Chem. Eng. J.* 152 (2009) 1–7.
- [8] A.B. dos Santos, F.J. Cervantes, J.B. van Lier, Review paper on current technologies for decolourisation of textile wastewaters: perspectives for anaerobic biotechnology, *Bioresour. Technol.* 98 (2007) 2369–2385.
- [9] G. Crini, P.M. Badot, Application of chitosan, a natural aminopolysaccharide, for dye removal from aqueous solutions by adsorption processes using batch studies: a review of recent literature, *Prog. Polym. Sci.* 33 (2008) 399–447.
- [10] S. Neatu, B. Cojocaru, V.I. Parvulescu, V. Somoghi, M. Alvaroc, H. Garcia, Visible-light C-heteroatom bond cleavage and detoxification of chemical warfare agents using titania-supported gold nanoparticles as photocatalyst, *J. Mater. Chem.* 20 (2010) 4050–4054.
- [11] H.Q. Sun, X.H. Feng, S.B. Wang, Combination of adsorption, photochemical and photocatalytic degradation of phenol solution over supported zinc oxide: effects of support and sulphate oxidant, *Chem. Eng. J.* 170 (2011) 270–277.
- [12] B. Bayarri, E. Carbonell, J. Gimenez, S. Esplugas, H. Garcia, Higher intrinsic photocatalytic efficiency of 2,4,6-triphenylpyrylium-based photocatalysts compared to  $\text{TiO}_2$  P-25 for the degradation of 2,4-dichlorophenol using solar simulated light, *Chemosphere* 72 (2008) 67–74.
- [13] V. Puddu, H. Choi, D.D. Dionysiou, G.L. Puma,  $\text{TiO}_2$  photocatalyst for indoor air remediation: influence of crystallinity, crystal phase, and UV radiation intensity on trichloroethylene degradation, *Appl. Catal. B* 94 (2010) 211–218.
- [14] X.L. Fu, X.X. Wang, Z.X. Ding, D.Y.C. Leung, Z.Z. Zhang, J.L. Long, W.X. Zhang, Z.H. Li, X.Z. Fu, Hydroxide  $\text{ZnSn}(\text{OH})_6$ : a promising new photocatalyst for benzene degradation, *Appl. Catal. B* 91 (2009) 67–72.
- [15] Y.F. Zhao, S. He, M. Wei, D.G. Evans, X. Duan, Hierarchical films of layered double hydroxides by using a sol-gel process and their high adaptability in water treatment, *Chem. Commun.* 46 (2010) 3031–3033.
- [16] A.I. Khan, D. O'Hare, Intercalation chemistry of layered double hydroxides: recent developments and applications, *J. Mater. Chem.* 12 (2002) 3191–3198.
- [17] K. Ladewig, M. Niebert, Z.P. Xu, P.P. Gray, G.Q.M. Lu, Efficient siRNA delivery to mammalian cells using layered double hydroxide nanoparticles, *Biomaterials* 31 (2010) 1821–1829.
- [18] F. Millange, R.I. Walton, L.X. Lei, D. O'Hare, Efficient separation of terephthalate and phthalate anions by selective ion-exchange intercalation in the layered double hydroxide  $\text{Ca}_2\text{Al}(\text{OH})_6 \cdot \text{NO}_3 \cdot 2\text{H}_2\text{O}$ , *Chem. Mater.* 12 (2000) 1990–1994.
- [19] J.B. Han, Y.B. Dou, M. Wei, D.G. Evans, X. Duan, Antireflection/antifogging coatings based on nanoporous films derived from layered double hydroxide, *Chem. Eng. J.* 169 (2011) 371–378.
- [20] B.M. Choudary, S. Madhi, N.S. Chowdari, M.L. Kantam, B. Sreedhar, Layered double hydroxide supported nanopalladium catalyst for heck-, suzuki-, sonogashira-, and stille-type coupling reactions of chloroarenes, *J. Am. Chem. Soc.* 124 (2001) 14127–14136.
- [21] B. Sels, D.D. Vos, M. Buntinx, F. Pierard, A.K.D. Mesmaeker, P. Jacobs, Layered double hydroxides exchanged with tungstate as biomimetic catalysts for mild oxidative bromination, *Nature* 400 (1999) 855–857.
- [22] Y.F. Zhao, M. Wei, J. Lu, Z.L. Wang, X. Duan, Biotemplated hierarchical nanostructure of layered double hydroxides with improved photocatalysis performance, *ACS Nano* 3 (2009) 4009–4016.
- [23] C.G. Silva, Y. Bouizi, V. Fornes, H. Garcia, Layered double hydroxides as highly efficient photocatalysts for visible light oxygen generation from water, *J. Am. Chem. Soc.* 131 (2009) 13833–13839.
- [24] W.Y. Shi, M. Wei, J. Lu, F. Li, J. He, D.G. Evans, X. Duan, Molecular orientation and fluorescence studies on naphthalene acetate intercalated  $\text{Zn}_2\text{Al}$  layered double hydroxide, *J. Phys. Chem. C* 112 (2008) 19886–19895.
- [25] E.A. Gardner, K.M. Huntoon, T.J. Pinnavaia, Direct synthesis of alkoxide-intercalated derivatives of hydroxalite-like layered double hydroxides: precursors for the formation of colloidal layered double hydroxide suspensions and transparent thin films, *Adv. Mater.* 13 (2001) 1263–1266.
- [26] J.H. Lee, S.W. Rhee, H.J. Nam, D.Y. Jung, Surface selective deposition of PMMA on layered double hydroxide nanocrystals immobilized on solid substrates, *Adv. Mater.* 21 (2009) 546–549.
- [27] S. Mandal, S. Mayadevi, Cellulose supported layered double hydroxides for the adsorption of fluoride from aqueous solution, *Chemosphere* 72 (2008) 995–998.
- [28] Z.P. Liu, R.Z. Ma, M. Osada, N. Iyi, Y. Ebina, K. Takada, T. Sasaki, Synthesis anion exchange, and delamination of Co-Al layered double hydroxide: assembly of the exfoliated nanosheet/polyanion composite films and magneto-optical studies, *J. Am. Chem. Soc.* 128 (2006) 4872–4880.
- [29] H.Y. Chen, F.Z. Zhang, S.S. Fu, X. Duan, In situ microstructure control of oriented layered double hydroxide monolayer films with curved hexagonal crystals as superhydrophobic materials, *Adv. Mater.* 18 (2006) 3089–3093.
- [30] S. He, Y.F. Zhao, M. Wei, X. Duan, Preparation of oriented layered double hydroxide film using electrophoretic deposition and its application in water treatment, *Ind. Eng. Chem. Res.* 50 (2011) 2800–2806.
- [31] Y. Zhao, F. Li, R. Zhang, D.G. Evans, X. Duan, Preparation of layered double hydroxide nanomaterials with a uniform crystallite size using a new method involving separate nucleation and aging steps, *Chem. Mater.* 14 (2002) 4286–4291.
- [32] H. Rousel, V. Briois, E. Elkaim, A. de Roy, J.P. Besse, Cationic order and structure of  $[\text{Zn}-\text{Cr}-\text{Cl}]$  and  $[\text{Cu}-\text{Cr}-\text{Cl}]$  layered double hydroxides: a XRD and EXAFS study, *J. Phys. Chem. B* 104 (2000) 5915–5923.
- [33] J.T. Klopogge, D. Wharton, L. Hickey, R.L. Frost, Infrared Raman study of inter-layer anions  $\text{CO}_3^{2-}$ ,  $\text{NO}_3^-$ ,  $\text{SO}_4^{2-}$ ,  $\text{ClO}_4^-$  in Mg/Al-hydroxalite, *Am. Mineral.* 87 (2002) 623–629.

- [34] J.W. Boclair, P.S. Braterman, One-step formation and characterization of Zn(II)-Cr(III) layered double hydroxides,  $Zn_2Cr(OH)_6X$  ( $X = Cl, 1/2SO_4$ ), Chem. Mater. 10 (1998) 2050–2052.
- [35] J.W. Boclair, P.S. Braterman, J. Jiang, S. Lou, F. Yarberry, Layered double hydroxide stability. 2. Formation of Cr(III)-containing layered double hydroxides directly from solution, Chem. Mater. 11 (1999) 303–307.
- [36] L.W. Zhang, Y.J. Wang, H.Y. Cheng, W.Q. Yao, Y.F. Zhu, Synthesis of porous  $Bi_2WO_6$  thin films as efficient visible-light-active photocatalysts, Adv. Mater. 21 (2009) 1286–1290.
- [37] Y.J. Li, S.G. Sun, M.Y. Ma, Y.Z. Ouyang, W.B. Yan, Kinetic study and model of the photocatalytic degradation of rhodamine B (RhB) by a  $TiO_2$ -coated activated carbon catalyst: effects of initial RhB content, light intensity and  $TiO_2$  content in the catalyst, Chem. Eng. J. 142 (2008) 147–155.
- [38] Z.P. Xu, G. Stevenson, C.Q. Lu, G.Q.M. Lu, Dispersion and size control of layered double hydroxide nanoparticles in aqueous solutions, J. Phys. Chem. B 110 (2006) 16923–16929.
- [39] H. Choi, E. Stathatos, D.D. Dionysiou, Sol-gel preparation of mesoporous photocatalytic  $TiO_2$  films and  $TiO_2/Al_2O_3$  composite membranes for environmental applications, Appl. Catal. B 63 (2006) 60–67.